Characterization of the sodium binding state in several food products by 23 Na nuclear magnetic resonance spectroscopy

Nour El Sabbagh, Jean-Marie Bonny, Sylvie Clerjon, Carine Chassain,
Guilhem Pagés

HAL Id: hal-03613378
https://hal.inrae.fr/hal-03613378v1

WILEY

Characterization of the sodium binding state in several food products by [23]Na nuclear magnetic resonance spectroscopy

Nour El Sabbagh[1,2,3] | Jean-Marie Bonny[1,2] | Sylvie Clerjon[1,2] | Carine Chassain[1,2,3] | Guilhem Pagés[1,2]

[1]UR QuaPA, INRAE, Saint-Gènes-Champanelle, France

[2]PROBE Research Infrastructure, AgroResonance Facility, INRAE, Saint-Genès-Champanelle, France

[3]CHU, CNRS, Clermont Auvergne INP, Institut Pascal, Université Clermont Auvergne, Clermont-Ferrand, France

Correspondence
Guilhem Pagés, INRAE, Route de Theix, 63122 Saint-Genès-Champanelle, France.
Email: guilhem.pages@inrae.fr

Abstract

In food, salt has several key roles including conservative and food perception. For this latter, it is well-known that the interaction of sodium with the food matrix modifies the consumer perception. It is then critical to characterize these interactions in various real foods. For this purpose, we exploited the information obtained on both single and double quantum [23]Na nuclear magnetic resonance (NMR) spectroscopies. All salted food samples studied showed strong interactions with the food matrix leading to quadrupolar interactions. However, for some of them, the single quantum analysis did not match the theoretical prediction. This was explained by the presence of another type of sodium population, which did not produce quadrupolar interactions. This finding is of critical importance to perform quantitative magnetic resonance imaging (MRI) and to understand the consumer salty taste perception.

KEYWORDS

[23]Na, multiple quantum coherences, NMR, relaxation time, salt concentration, T_2 amplitude

1 | INTRODUCTION

The role of salt in food is multiple. It contributes to the product sensory properties and is also a key molecule regarding the food structural and stability characteristics. However, its consumption must be limited to avoid health issues as highlighted by several international agencies.[1] From the consumer point of view, this salt content reduction should not be associated with a decrease of salty expected taste. The taste buds leading to the saltiness feeling are sensitive to the sodium ions released from the sodium chloride. Once the solid food is eaten (i.e., into the mouth of the consumer), several complex processes are taking place leading at the end to the perception of the saltiness. They can be merged into three main actions.[2] First, the salt is migrating to the surrounding part of the bolus food particles. Then, the

sodium ions are released into the oral cavity through the saliva. Finally, sodium ions reach the tongue's taste receptor cells generating a series of activations in the brain which conduct to the sensation of saltiness.[3] Sodium ions binding with the food matrix is one of the critical parameters, which may be correlated with saltiness perception. For example, products containing a same amount of salt but a higher quantity of dry matter or protein were felt less salty[4–7] because the salt released from the matrix was reduced. The complexity and composition variability of food products make it difficult to correlate saltiness to a global food characteristic, highlighting the importance of having information on the salt local repartition.

[23]Na magnetic resonance imaging (MRI) appears as a technique of choice to characterize the repartition and the interaction of sodium with the matrix. One of
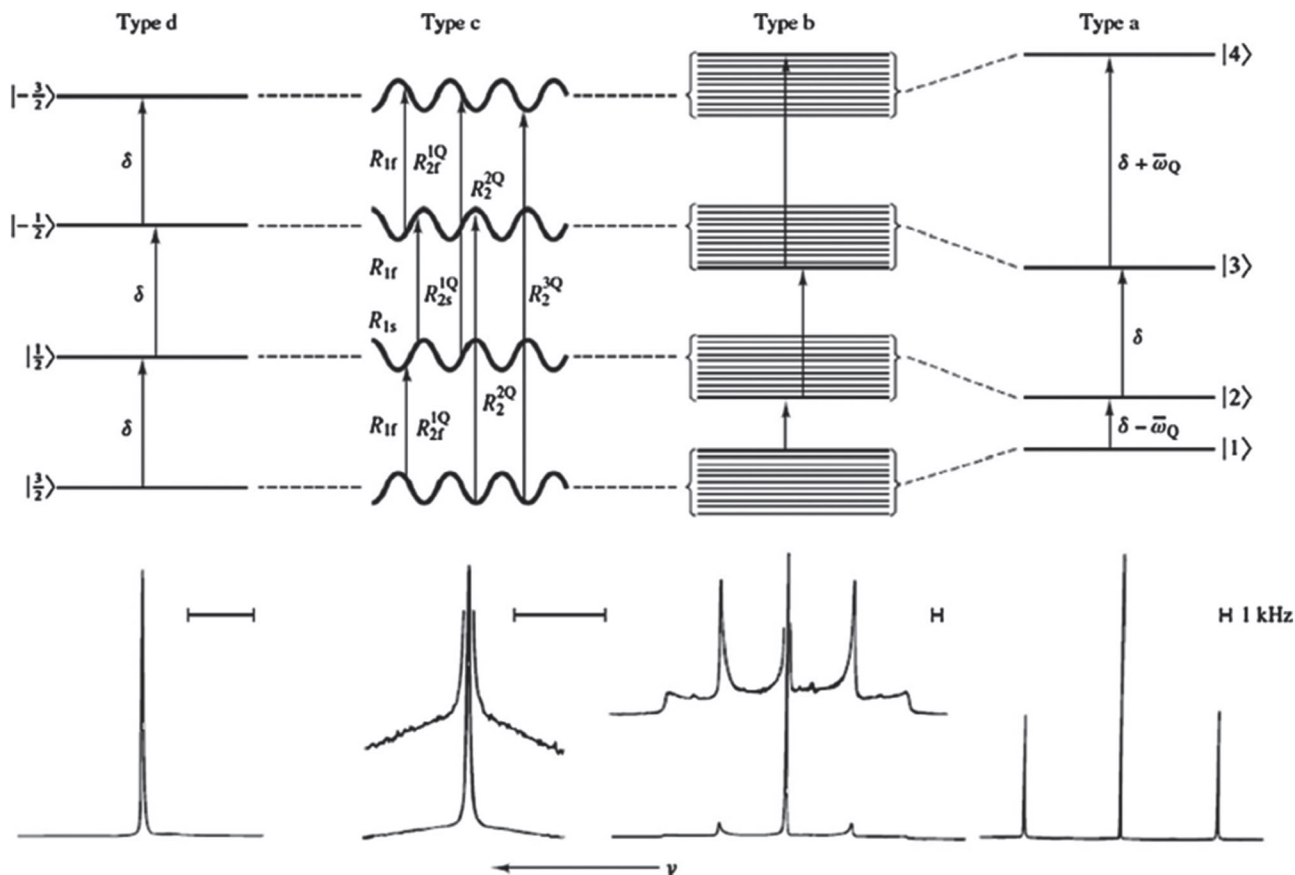
FIGURE 1 Energy level diagrams for isolated systems of spin 3/2. Four different motional regime situations are possible (**a**, **b**, **c**, and **d**). ^{23}Na spectra corresponding to each situation are presented: Type **d** spectrum was that of NaCl in H_2O. Type **c** spectrum was that of Na^+ in an aqueous solution which has a high concentration of micelle-solubilized gramicidin channels. The type **b** and type **a** spectra were that of Na^+ in aqueous suspensions of un-oriented and oriented dodecylsulfate micelles, respectively. Reproduced with permission from Rooney and Springer[23]
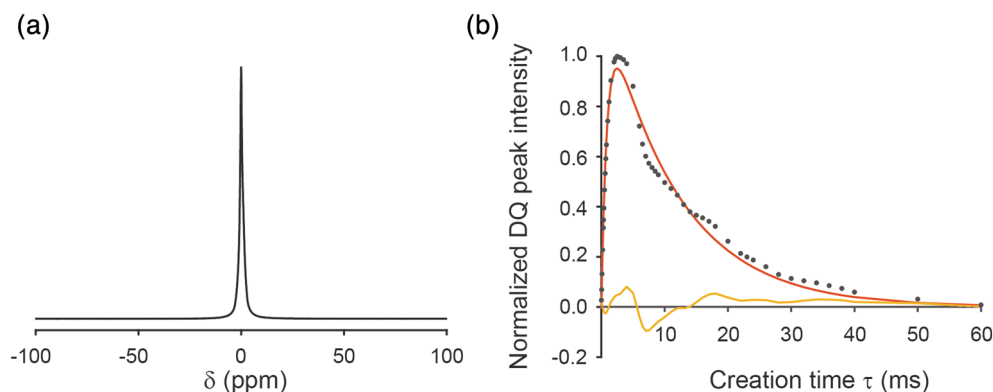
FIGURE 2 Trout (a) SQ ^{23}Na spectrum and (b) DQ-filtered ^{23}Na peak intensity evolution in function of the creation time. Data were fitted according to Equation 1 (red curve) and the residuals were plotted in orange

the first work in this field studied the sodium repartition during the pickling of a cucumber in a fermented soybean paste.[8] ^{23}Na MRI was combined with other nuclear magnetic resonance (NMR) approaches to study the salting/desalting process of salmon[9,10] and cod[11] for several muscle conditions (e.g. frozen vs. thawed) or to characterize meat curing.[12] ^{23}Na MRI helped also in understanding how subcutaneous fat can limit the salt diffusion[13] or what is the importance of the salting method (brine injection with or without an adjuvant vs pickle) on the repartition of salt inside the muscle.[14] Most of these works target to map the sodium concentration in food to better control the effect of processes on this repartition. However,

TABLE 1 Fast and slow T_2 relaxation times and normalized population fractions resulting from the fitting of the ^{23}Na DQF spectra

Food matrix	$T_{2,F}^{DQ}$ (ms)	$T_{2,S}^{DQ}$ (ms)	A_F^{DQ}	A_S^{DQ}
Trout	0.9 ± 0.1	11.5 ± 0.9	0.50 ± 0.03	0.50 ± 0.03
Pasta	0.8 ± 0.1	6.1 ± 0.4	0.50 ± 0.03	0.50 ± 0.03
Chicken	1.4 ± 0.2	14.1 ± 1.2	0.50 ± 0.04	0.50 ± 0.04
Carrot	0.6 ± 0.1	22.8 ± 2.5	0.50 ± 0.06	0.50 ± 0.03

Note: Results for the salted trout and for the pasta, chicken and carrot cooked in water with a salt concentration of 20 g/L.
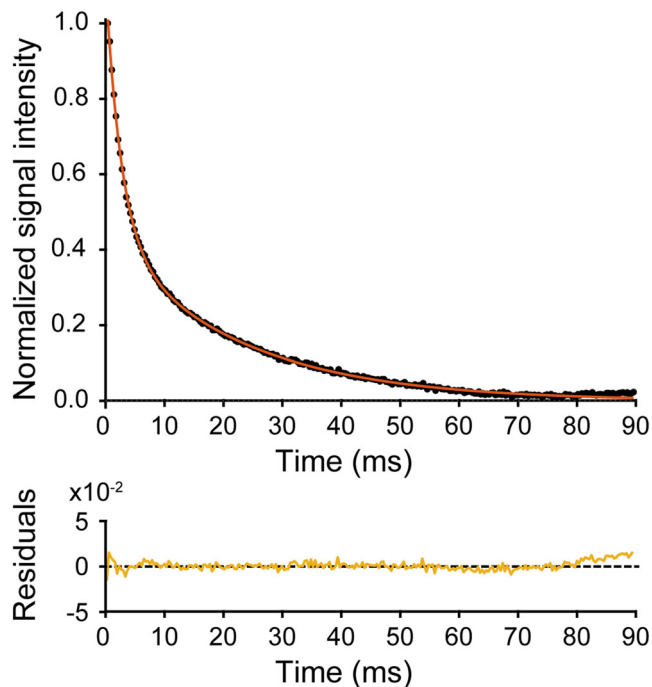

FIGURE 3 Trout ^{23}Na SQ Carr–Purcell–Meiboom–Gill (CPMG) echoes (black dots) and fitted curve (red line) according to Equation 2. The subplot represents the residuals

there is a lack of knowledge on the bounding state of such ions in real foods. ^{23}Na relaxation times can be really short (few milliseconds) and, in consequence, difficult to detect—and a fortiori complicated to quantify—by MRI. Furthermore, difference of relaxations may modulate the saltiness perception. It is then necessary to study the food sample as a whole for performing thorough ^{23}Na NMR relaxation studies and characterize all the sodium pools.

^{23}Na NMR relaxometry has been used to characterize several food matrices. For example, the relationship between sodium properties and the structure and composition of cheese had been extensively studied.[15,16] Similarly, the sodium mobility was characterized in an emulsion gel model.[17] Sodium mobility deduced by NMR was also correlated with saltiness perception. One of the first study demonstrated that the sodium mobility in gums was positively correlated with saltiness

perception.[18,19] Boisard et al. correlated the sodium ions release in the oral cavity (and so to the saltness perception) to the lipid/protein ratio.[19] In another study, Mosca et al. did a similar study on cheese model matrices.[20] The sodium mobility was in general an indirect measurement through the T_2 relaxation times. Recently Wang et al. proposed to directly use NMR diffusion measurements to correlate the sodium mobility with the saltiness perception.[21]

The sodium mobility and its binding to the solid part of the food have been characterized only for a few real systems. Gaining a deeper knowledge on the sodium state in several food products is critical before going to quantitative NMR/MRI-based methods. The aim of this paper is to characterize the sodium state in contrasted food products by single quantum (SQ) and double quantum (DQ) ^{23}Na NMR spectroscopy. To accurately interpret our results, we will detail and explain the different energy level configurations which can be encountered in ^{23}Na NMR and describe the experimental strategy implemented.

2 | THEORY AND EXPERIMENTAL STRATEGY

Sodium nucleus has a nuclear spin of 3/2, which leads to quadrupolar interactions between the charges in the nucleus and the surrounding electric field gradients (EFG). The equal transitions between the four nuclear spin energy levels become unequal under the effect of these quadrupolar interactions. At the macroscopic observation scale, the NMR spectra depends on how these interactions are averaged with time for a large number of spins. Indeed, EFG fluctuates in time due to molecular motion. For a deeper analysis, the interested reader is referred to the excellent review by Madelin et al.[22]

Figure 1 illustrates the four different motional regime situations, each leading to a typical SQ spectrum. The different situations are related to the EFG fluctuation frequency in regards of the NMR timescale and are classified following Rooney and Springer

Food matrix	$T_{2,F}^{SQ}$ (ms)	$T_{2,S}^{SQ}$ (ms)	A_F^{SQ}	A_S^{SQ}	SNR
Trout	2.7 ± 0.1	22.4 ± 0.3	0.61 ± 0.01	0.39 ± 0.01	34.09
Pasta	2.7 ± 0.1	30.7 ± 1.9	0.80 ± 0.02	0.21 ± 0.01	6.06
Chicken	3.1 ± 0.2	21.9 ± 1.5	0.67 ± 0.03	0.34 ± 0.03	3.72
Carrot	4.4 ± 0.8	25.2 ± 2.2	0.46 ± 0.05	0.54 ± 0.05	2.90

TABLE 2 Fast and slow T_2 relaxation times and normalized population fractions resulting from the fitting of the SQ Carr–Purcell–Meiboom–Gill (CPMG) ^{23}Na data

Note: The SNR is also reported for all samples. Results for the salted trout and for the pasta, chicken and carrot cooked in water with a salt concentration of 20 g/L are presented.
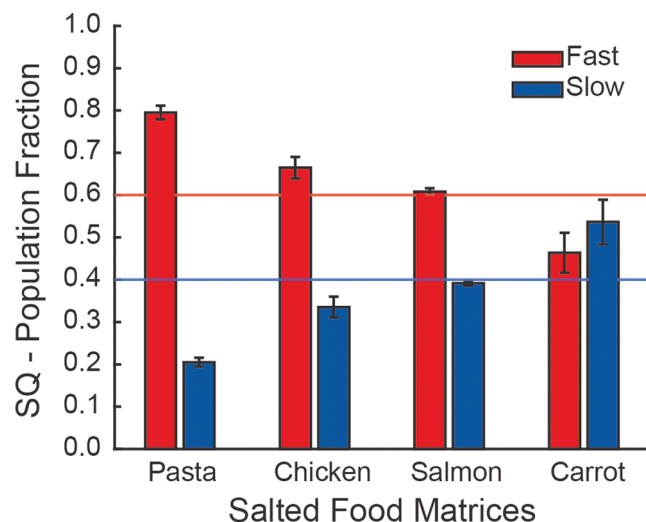

FIGURE 4 Fast and slow population fractions extracted from the SQ Carr–Purcell–Meiboom–Gill (CPMG) fitting curve for the smoked salmon and for the pasta, chicken and carrot cooked in water with a salt concentration of 20 g/L. The lines represented the theoretical fractions

central narrow peak and a frequency distribution for the outer ones. The fourth case appears when the EFG variations are similar to the NMR timescale. In this case, the energy level differences stay constant (type **d**) with a fluctuation around the averaged value. This is the type **c** (Figure 1). The NMR spectrum of this situation corresponds to a narrow peak for the central line overlapped with a broad signal for the outer energy levels. By recording a DQ or triple quantum filtered (DQF, TQF) NMR spectrum, only sodium presenting quadrupolar interactions leads to a signal. Regarding the different situations described, sodium of type **a**, **b**, and **c** gives rise to a signal while type **d** does not give any signal.

The transverse relaxation time T_2 can help to characterize the different spectrum types. Let first describe the SQ T_2 relaxation. For type **a** in which the quadrupolar effect is well defined, a mono-exponential decay is observed for each of the three NMR signals. The central line has a longer T_2 than the two outer peaks, which have the same relaxation time. At the opposite, type **d** spectrum is characterized by a mono-exponential decay as ω_q is null and the motion is isotropic with motional narrowing. For slower motional regimes, i.e. type **c** in Figure 1, a bi-exponential behavior is observed characterizing the central and satellite transitions for the slow and fast relaxation times, respectively. Furthermore, their amplitudes can be predicted to be 2/5 and 3/5 for the inner and outer transitions, respectively. Considering the DQ T_2 analysis, only two coherences exist with an equal probability. It is expected to obtain a fast and a slow DQ T_2 relaxation time contributing to the same percentage to the NMR signal.

Based on this knowledge, we used the following approach to characterize the sodium interactions into the food matrices. First, a SQ spectrum was analyzed to determine if the interactions were of type either **a**, **b** or **c**, **d**. As type **c** and **d** could not be differentiate from their SQ spectra, DQF data were acquired. The presence of a DQ signal highlighted the presence of type **c** quadrupolar interactions with the food matrix. DQ T_2 relaxation parameters were calculated to confirm the presence of two equal populations. Finally, SQ T_2 signal decay was analyzed by using a bi-exponential model. If the

proposition.[23,24] The effect of this EFG is expressed in the quadrupolar coupling angular frequency term ω_q averaged over time and space. For very fast EFG variations, ω_q is null leading to the situation annotated type **d** in Figure 1. This is typically observed for sodium nuclei in solution and a single NMR peak, which merges all the transitions, is then observed in the frequency domain. At the opposite, in type **a** (Figure 1), the EFG term is well-defined and different from 0 leading to a difference between the energy levels depending on ω_q. This is only observed in few oriented and spatially homogeneous solid samples.[25] In this case, a triplet of intensities 3:4:3 is observed in the NMR spectrum with chemical shifts of δ for the center line and $\delta \pm \overline{\omega}_q$ for the outer ones. In between these two cases, it exists two intermediate situations. Type **b** (Figure 1) corresponds to a less oriented medium. The EFG varies slowly on the NMR timescale leading to a non-null but fluctuating ω_q. The energy levels are still shifted but they are distributed over a range of levels. In term of NMR spectra, this leads to a

TABLE 3 DQ and SQ ^{23}Na relaxation results for the pasta and carrot samples cooked in water with different salt concentrations

| Food matrix	[salt] (g/L)	DQ				SQ			
		$T_{2,F}^{DQ}$ (ms)	$T_{2,S}^{DQ}$ (ms)	A_F^{DQ}	A_S^{DQ}	$T_{2,F}^{SQ}$ (ms)	$T_{2,S}^{SQ}$ (ms)	A_F^{SQ}	A_S^{SQ}
Pasta	10	0.8 ± 0.2	6.9 ± 1.2	0.51 ± 0.08	0.50 ± 0.08	3.0 ± 0.2	27.4 ± 1.5	0.70 ± 0.02	0.30 ± 0.02
	20	0.8 ± 0.1	6.1 ± 0.4	0.50 ± 0.03	0.50 ± 0.03	2.7 ± 0.1	30.7 ± 1.9	0.80 ± 0.02	0.21 ± 0.01
Carrot	5	—	—	—	—	4.9 ± 1.0	25.3 ± 3.3	0.51 ± 0.07	0.49 ± 0.08
	10	0.4 ± 0.1	25.6 ± 3.7	0.51 ± 0.08	0.49 ± 0.03	3.4 ± 0.5	21.9 ± 1.4	0.46 ± 0.04	0.54 ± 0.04
	15	0.8 ± 0.2	28.5 ± 3.1	0.50 ± 0.05	0.50 ± 0.03	3.8 ± 0.6	23.4 ± 1.2	0.39 ± 0.03	0.61 ± 0.04
	20	0.6 ± 0.1	22.8 ± 2.5	0.50 ± 0.06	0.50 ± 0.03	4.4 ± 0.8	25.2 ± 2.2	0.46 ± 0.05	0.54 ± 0.05
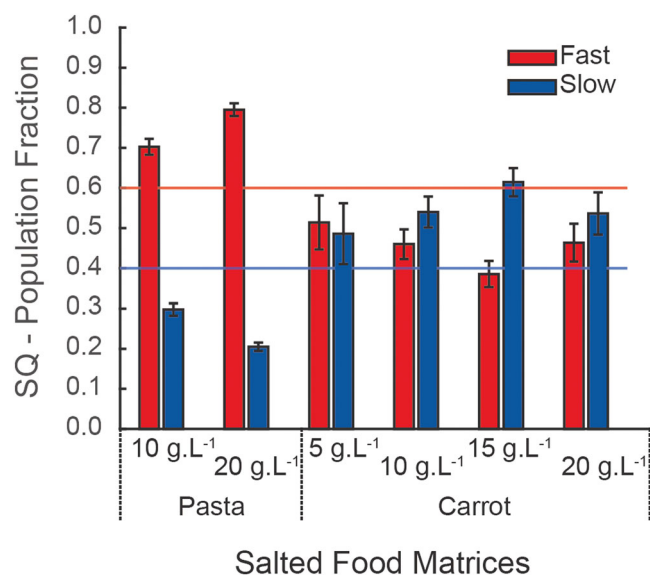
FIGURE 5 Effect of the salt concentration on the SQ fast and slow fraction values for both the pasta and carrot. The lines were drawn at the theoretical fraction values

amplitudes were 3/5 and 2/5 for the fast and slow relaxation times, respectively, we considered that 100% of the sodium was of type **c**. A difference from these theoretical values suggested the presence of an additional fraction of free sodium of type **d**.

3 | RESULTS AND DISCUSSION

3.1 | Characterization of different food

At first, we studied different food samples (pasta, chicken and carrot) cooked in a salted water (20 g/L) alongside salted trout. For the different food matrices, the SQ ^{23}Na FID provided only one-peak as illustrated for the trout ^{23}Na SQ spectrum (Figure 2a). This eliminated the possibility of having ^{23}Na pools of type **a** or **b** because of the

absence of lateral and symmetric peaks around the central bulk one. However, multiple pools of type **d** could be confused with a pool of type **c**. Considering that only type **c** carries DQ coherences because of significant dynamic quadrupolar effects, a DQF experiment allowed ascertaining the presence or not of type **c** interactions. Figure 2b shows the evolution of the DQF signal intensity with the creation time on the trout (black dots). This signal evolution can be fitted according to Equation 1 to estimate the two relaxation times and their amplitudes. This fitting as well as the residuals are represented on Figure 2b (red and orange lines, respectively). The model did not perfectly match the experimental data as there are some oscillations. These DQF NMR spectra presented a good SNR (i.e. >450 at the optimal creation time) suggesting that these variations cannot be ascertained to noise. One hypothesis is few sodium type **c** pools existed complexifying the relaxation analysis. However, resolving such minor pools is currently too challenging. The resulting relaxation times and amplitude fractions are summarized in Table 1. All samples led to a DQ NMR spectrum giving a first evidence of the presence of type **c** sodium. An equal fraction between both fast and slow populations was found for the different matrices in agreement with what was expected from the theory. This demonstrated that sodium quadrupolar interactions of type **c** were clearly detectable in the different salted food matrices.

Figure 3 represents the SQ Carr–Purcell–Meiboom–Gill (CPMG) bi-exponential fitting for the trout. It shows that this model matches the signal decay. Furthermore, the residuals were carefully visually checked to validate the fit quality. For all the samples, no significant deviations of the residuals was detected. When only a type **c** is present and by using such model, the amplitude of fast and slow components should be 3/5 and 2/5, respectively. Obtaining different amplitude values would highlight the presence of type **d** sodium. The fitting results for the different food matrices are summarized in Table 2 and

TABLE 4 Sample preparation details

Food sample	Volume of cooking water (mL)	[Salt] of the cooking water (g/L)	Cooking time (min)	Weight of the sample (g)		
				Prior cooking	Post cooking	In the NMR tube
Pasta	500	10.11	9	20.84	—	0.18
	250	20.04		3.72	7.87	0.16
Chicken	250	20.32	7	6.94	4.88	0.12
Carrot	250	5.00	10	6.65	6.21	0.24
		10.01		6.73	6.25	0.23
		15.01		6.67	6.20	0.30
		20.05		6.77	6.20	0.30

TABLE 5 Main parameters of the SQ (FID, CPMG) and DQ experiments

Food Matrix	[Salt] of the cooking water (g/L)	SQ			DQF
		FID		CPMG[a]	
		NS[b]	TD[b]	NS[b]	TD[b]
Trout	—	20	2048	1600	2048
Pasta	10	40	1024	4600	2048
	20	20	4096	8000	4096
Chicken	20	70	2048	8600	4096
Carrot	5	100	4096	8600	4096
	10			6500	
	15			8000	
	20			6800	

[a]The Carr–Purcell–Meiboom–Gill (CPMG) was recorded with 256 echoes obtained every 175 μs. Only one data point per echo was recorded and calculated by the mean value of the 8 data point intensity around the echo. The CPMG experiments were not phase-cycled as neither offset nor pulse imperfection artifacts were observed.

[b]NS = number of scans; TD = number of points of the FID.

Figure 4. For the salted trout, the relative fractions were found as 3/5 and 2/5 with transverse relaxation times of 2.7 and 22.4 ms for the fast and slow components, respectively. Combining these SQ results with the DQ ones, we concluded that the whole sodium population in the salted trout was of type **c**. The amplitudes estimated for the salted chicken were close to the predicted ones suggesting that almost all the sodium experienced quadrupolar interactions. Regarding the pasta and carrot, the measured population fractions between fast and slow components were far from the expected values in the presence of only type **c**. The significant differences from the theoretical values demonstrated the presence of free sodium of type **d** for both salted pasta and carrot samples.

Because of the strong evidence of having two different pools of sodium of type **c** and **d** in the latter food samples, such system should ideally be fitted with a three-exponential model: two components belonging to the type **c** sodium and one for the type **d**. The sodium T_2 relaxation time in water was measured to 53 ms at a concentration of 20 g/L. To be able to resolve this model with such narrow relaxation range, it is critical to have high-SNR data, i.e. higher than 1000 for three exponentials.[26] Unfortunately, our experimental conditions were far to reach a sufficient SNR (see Table 2), which appears challenging considering the sodium sensitivity.

3.2 | Effect of the salt concentration on the sodium interactions

To strengthen our analysis, we studied the pasta and carrot samples for different salt concentrations as a variation of the quantity of type **c** and type **d** was expected. The SQ and DQ results are summarized in Table 3. DQ fitting

was not performed for the carrot cooked in 5 g/L salted water because the signal detected was too low. DQ experiments showed equal fractions for both fast and slow populations for all samples as expected. This confirmed the presence of the sodium of type **c** for the different salt concentrations.

Figure 5 shows the amplitudes for each of the two SQ relaxation components and for each food and salt concentration. For the pasta samples, the fast population fraction increased with the increase of the salt concentration while it is the slow population fraction which increased for the carrot samples. An interpretation would be that a pool of free sodium (type **d**) was detected with an increase of its fraction with the cooking water salt concentration. However, it is not the same fraction which increased for the different food. Because the model describing the data cannot be complexified (explained previously), at this stage we can only speculate to explain the apparent contradictory population fraction evolution. The type **d** relaxation time value is not known in the different food samples and it can only be assumed lower than this one measured in the salted water solution (53 ms). Furthermore, depending on its value, this component can merge with either the fast or the slow component of the bi-exponential model. The type **d** T_2 in the pasta is shorter than this one in the carrot and merged with the fast component of the model while the carrot type **d** T_2 merged with the slow component. Furthermore, we cannot exclude that both sodium populations are exchanging leading to a relaxation decay analysis significantly more complex.[27] A change in the exchange rate between the sodium pools in both food products might also explained the difference in the relaxation fractions observed in Figure 5. Finally, we can note a decrease of the slow fraction for the most salted carrot sample. It is difficult to assign this evolution change to possible experimental issues or to a change in the evolution of the system (e.g., change in type **d** T_2 value, in the type **c** and **d** fractions).

Although the DQ study demonstrated the presence of sodium quadrupolar interactions of type **c** for the different salted matrices; the relaxation times, their relative amplitude fractions, and their evolution with the salt concentrations were diverse. Additionally, the salt concentration gradients in the same food matrix, leading to different relaxation times, cannot be ignored. This can be studied through imaging techniques. However, it is difficult to obtain the same accuracy as the analysis presented in this work because it is almost impossible to obtain readily a narrow echo time sampling. To tackle this problem, one possible solution would be to sample the food at different locations and to perform the same spectroscopy study as this one described in this article.

4 | CONCLUSIONS

This work was a proof of concept that different sodium pools may coexist in food matrices. Indeed, the sodium interactions in food are complex with a combination of type **c** and type **d** sodium. The characterization of the sodium type is critical to quantify it and to understand the relationship with the salted taste. While type **c** can readily be detected by a multi-quanta filter (here a DQF), the presence of type **d** is only indirectly demonstrated. It would be interesting to run a pulse sequence displaying the signal of only the spins which do not have quadrupolar interactions. To the best of our knowledge, such sequence does not exist. In this study, we did not measure the T_1 longitudinal relaxation recovery. In clinical application,[28] a significant T_1 contrast was highlighted for different type **c** sodium pools. It deserves to be studied to evaluate its capability to separate the different sodium compartments in our context.

These preliminary results deserve further investigation by repeating the experiments to consider the inter-matrix variability. A larger range of salt concentrations may help to study the evolution of the sodium pools behavior with the food. Other types of food can be examined to investigate the dependence of the quadrupolar interactions with various matrices. For proper salt quantification, it is critical to have an excellent knowledge of the different sodium pools.

5 | MATERIAL AND METHODS

5.1 | Sample preparation

In our work, we studied several food with different salting processes. The first one was a farmed trout salted filet (*Oncorhynchus mykiss*). The filet weighted 589 g and was salted with 6% in weight of dry salt on the internal filet face during 3.5 h at 8°C. After the salting period, it underwent 6 h at 24°C to simulate the smoking period (water loss) and was then stored at 5°C. A 16-g sample was placed in a 30-mm (50 mL) Falcon tube for NMR experiments (as such tube fitted well in the insert).

Three other food samples were cooked in salted water: a piece of a chicken breast, carrots and Tagliatelle pasta. First, each food sample was placed in a salted boiling water for a duration sufficient for being properly stewed. After cooking, the food sample was placed in the fridge to cool for 15 min. A small amount of each sample was inserted in a 5-mm NMR tube. Table 4 summarizes the experimental conditions for the different samples.

5.2 | Nuclear magnetic resonance experiments

All experiments were performed on a 9.4 T Bruker UltraShielded widebore magnet (Karlsruhe, Germany) equipped with Avance III electronics and piloted by Top-Spin 3.5. The magnet reference resonance frequencies were 400.18 and 105.86 MHz for ^1H and ^{23}Na, respectively. $^1H/^{23}Na$ volume coils were used to excite and receive both nuclei. A 30-mm insert (Bruker BioSpin, Karlsruhe, Germany) was used for the trout, and a 5-mm broadband observe (BBO) probe (Bruker BioSpin, Karlsruhe, Germany) for the other samples. Once the sample was inserted inside the spectrometer, the first step consisted in adjusting the magnetic field homogeneity based on a ^1H spectrum. Then, the ^{23}Na 90° pulse length was calibrated. It was found to be around 88 μs at 280 W and 9 μs at 50 W for the 30-mm insert and the BBO probe, respectively. Finally, SQ and DQ ^{23}Na experiments were run. The repetition time was set to 0.5 s and the receiver gain to 256 for all experiments. The repetition time was set accordingly to the T_1 values found in the literature (i.e., <0.1 s; e.g., previous works[15-17,19,28]). The main parameters of the experiments are presented in Table 5. DQ coherences were selected using the phase-cycled pulse sequence below

$$(\pi/2)_{\varphi_1} - \tau/2 - (\pi)_{\varphi_2} - \tau/2 - (\pi/2)_{\varphi_1} - \delta - (\pi/2)_{\varphi_3}$$
$$- Acq(t)_{\varphi'},$$

where τ is the DQ creation time and δ, the DQ evolution time. The basic four-step phase cycle of the sequence to eliminate SQ coherences was: $\varphi_1 = 0°, 90°, 180°, 270°$; $\varphi_2 = \varphi_1 + 90°$, $\varphi_3 = 0°$ and $\varphi' = 0°, 180°, 0°, 180°$.[29] This DQF was applied with 4 μs evolution time (δ) and for several creation time (τ) duration, ranging from 0 to 120 ms.

5.3 | Data processing

All experiments were fitted by using MATLAB® R2020a (MathWorks, Natick, MA, USA). Several DQ NMR data were acquired with different creation times. The DQ peak intensity of each spectrum was extracted and fitted by the following bi-exponential expression

$$A_S^{DQ} \exp(-\tau/T_{2,S}^{DQ}) - A_F^{DQ} \exp(-\tau/T_{2,F}^{DQ}). \quad (1)$$

where $T_{2,S}^{DQ}$ and $T_{2,F}^{DQ}$ are the slow and fast DQ relaxation times, respectively, and A_S^{DQ} and A_F^{DQ} their corresponding

amplitudes. To analyze the SQ CPMG data, the noise level was calculated by calculating the standard deviation of the last points. The CPMG data were fitted until the signal decayed down to 3 times the noise with the following bi-exponential model

$$A_S^{SQ} \exp(-t/T_{2,S}^{SQ}) + A_F^{SQ} \exp(-t/T_{2,F}^{SQ}). \quad (2)$$

where $T_{2,S}^{SQ}$ and $T_{2,F}^{SQ}$ are the slow and fast SQ relaxation times and A_S^{SQ} and A_F^{SQ} their corresponding amplitudes.

ORCID

Nour El Sabbagh https://orcid.org/0000-0001-5100-3429
Jean-Marie Bonny https://orcid.org/0000-0003-2858-7459
Sylvie Clerjon https://orcid.org/0000-0002-6273-200X
Carine Chassain https://orcid.org/0000-0002-9234-2344
Guilhem Pagés https://orcid.org/0000-0001-9368-5237

REFERENCES

[1] *Global action plan for the prevention and control of non-communicable diseases 2013–2020*, World Health Organization **2013**.

[2] W. Y. Kuo, Y. S. Lee, *Compr. Rev. Food Sci. Food Saf.* **2014**, *13*(5), 906.

[3] T. Kobayakawa, S. Saito, N. Gotow, H. Ogawa, *Chemosens. Percept.* **2008**, *1*(4), 227.

[4] F. J. Colmenero, M. J. Ayo, J. Carballo, *Meat Sci.* **2005**, *69*(4), 781.

[5] M. Ruusunen, J. Vainionpää, M. Lyly, L. Lähteenmäki, M. Niemistö, R. Ahvenainen, E. Puolanne, *Meat Sci.* **2005**, *69*(1), 53.

[6] C. Lauverjat, I. Deleris, I. C. Trelea, C. Salles, I. Souchon, *J. Agric. Food Chem.* **2009**, *57*(21), 9878.

[7] M. Panouille, A. Saint-Eve, C. de Loubens, I. Deleris, I. Souchon, *Food Hydrocolloids.* **2011**, *25*(4), 716.

[8] N. Ishida, T. Kobayashi, H. Kano, S. Nagai, H. Ogawa, *Agric. Biol. Chem.* **1991**, *55*(9), 2195.

[9] I. G. Aursand, U. Erikson, E. Veliyulin, *Food Chem.* **2010**, *120*(2), 482.

[10] I. G. Aursand, E. Veliyulin, U. Bocker, R. Ofstad, T. Rustad, U. Erikson, *J. Agric. Food Chem.* **2009**, *57*(1), 46.

[11] U. Erikson, E. Veliyulin, T. E. Singstad, M. Aursand, *J. Food Sci.* **2004**, *69*(3), E107.

[12] H. C. Bertram, S. J. Holdsworth, A. K. Whittaker, H. J. Andersen, *J. Agric. Food Chem.* **2005**, *53*(20), 7814.

[13] L. Gallart-Jornet, J. M. Barat, T. Rustad, U. Erikson, I. Escriche, P. Fito, *J. Food Eng.* **2007**, *79*(1), 261.

[14] M. Gudjonsdottir, A. Traore, A. Jonsson, M. G. Karlsdottir, S. Arason, *Food Chem.* **2015**, *188*, 664.

[15] L. Boisard, I. Andriot, C. Arnould, C. Achilleos, C. Salles, E. Guichard, *Food Chem.* **2013**, *136*(2), 1070.

[16] M. Gobet, L. Foucat, C. Moreau, in *Investigation of Sodium Ions in Cheeses by ^{23}Na NMR Spectroscopy*, (Eds: M. Guojonsdottir, P. Belton, G. Webb), Royal Soc Chemistry, Cambridge **2009**, 57.

[17] K. S. Okada, Y. Lee, *J. Food Sci.* **2017**, *82*(7), 1563.

[18] T. R. Rosett, L. Shirley, S. J. Schmidt, B. P. Klein, *J. Food Sci.* **1994**, *59*(1), 206.

[19] L. Boisard, I. Andriot, C. Martin, C. Septier, V. Boissard, C. Salles, E. Guichard, *Food Chem.* **2014**, *145*, 437.

[20] A. C. Mosca, I. Andriot, E. Guichard, C. Salles, *Food Hydrocolloids* **2015**, *51*, 33.

[21] X. J. Wang, X. W. Wang, T. T. Feng, Y. Shen, S. Q. Xia, *Food Chem.* **2021**, *347*, 9.

[22] G. Madelin, J. S. Lee, R. R. Regatte, A. Jerschow, *Prog. Nucl. Magn. Reson. Spectrosc.* **2014**, *79*, 14.

[23] W. D. Rooney, C. S. Springer, *NMR Biomed.* **1991**, *4*(5), 209.

[24] W. D. Rooney, C. S. Springer, *NMR Biomed.* **1991**, *4*(5), 227.

[25] M. D. Meadows, K. A. Smith, R. A. Kinsey, T. M. Rothgeb, R. P. Skarjune, E. Oldfield, *Proc. Natl. Acad. Sci. U. S. a.* **1982**, *79*(4), 1351.

[26] N. J. Clayden, B. D. Hesler, *J. Magn. Reson.* **1992**, *98*(2), 271.

[27] T. E. Bull, *J. Magn. Reson.* **1972**, *8*(4), 344.

[28] G. Madelin, A. Jerschow, R. R. Regatte, *NMR Biomed.* **2012**, *25*(4), 530.

[29] R. KempHarper, S. P. Brown, C. E. Hughes, P. Styles, S. Wimperis, *Prog. Nucl. Magn. Reson. Spectrosc.* **1997**, *30*, 157.